Query Details

Back to Main Page

1. Please check and confirm the edit made in the article title.

2. Please confirm if the corresponding author is correctly identified. Amend if necessary.

3. Please check edit "...it is assumed that either the whole ray path is along..." The word "either" was used, implying that "or" was needed instead of "and." Amend if needed.

4. Please check edits to Fig. 9 caption, and amend as needed.

Depth-Dependent Shear-Wave Attenuation in Central Apennines, Italy

Raúl R. Castro
Email : raul@cicese.mx
Francesca Pacor
Email : francesca.pacor@ingv.it
Daniele Spallarossa
Email : daniele@dipteris.unige.it

División Ciencias de la Tierra, Departamento de Sismología, Centro de Investigación Científica y de Educación Superior de Ensenada (CICESE), 22860, Ensenada, Baja California, Mexico

Istituto Nazionale di Geofísica e Vulcanologia, Sezione di Milano, Milan, Italy

Universita degli Studi di Genova, DISTAV, Genova, Italy

Received: 20 July 2020 / Accepted: 24 April 2021

Abstract

We used 1029 earthquakes, AQ1 with magnitudes ranging from M 3.0 to M 6.5, located in central Apennines, Italy, and recorded by 414 local stations to study the variation of the quality factor Q_S of shear waves with depth. We first determined average nonparametric attenuation functions in the frequency band from 0.5 to 20 Hz and hypocenter distances less than 155 km to correct the observed acceleration spectra for attenuation effects. Then, we separated source and site effects from the corrected spectral records to determine the changes of Q_S with depth. We used a 1D local shear-wave velocity model to calculate the travel times of the source-station paths, and we inverted the observed spectra to determine Q_S in three different depth intervals (0–4 km, 4–10 km and 10–15 km) and five frequencies (0.5, 1, 4, 10 and 20 Hz). We found that Q_S increases with frequency AQ2 at all depths considered and tends to have lower values at shallow depths. The average value of Q_S is consistent with previous studies made in central Italy and can be approximated by $Q_S = 43f^{0.94}$. To describe the frequency dependence of Q_S with depth (H), we determine the following relations: $Q_S = 5.5f^{1.39}$, $0.5 \leq f \leq 10$ Hz and $Q_S = 151.5$, $f > 10$ Hz for 0–4 km, $Q_S = 52f^{0.87}$ for $4 < H < 10$ km and $Q_S = 51f^{0.92}$ for $10 \leq H \leq 15$ km. We conclude that the Q-depth-dependent model can be useful to improve estimates of source parameters and ground motion prediction in the central Apennines region of Italy.

Keywords

Central Italy
seismic attenuation
quality factor

1. Introduction

In central Italy (latitude 41 N–43 N and longitude 12 E–15 E), where the regions of Abruzzo, Umbria and Marche are located, active faults generate damaging earthquakes, having magnitudes as high as M_w 7 like the earthquake that occurred in 1915 (Avezzano, 1915). The seismicity in this region results from the collision between the African and the European continental margins (Alvarez et al., 1974; Pauselli

generate long earthquake sequences like the recent sequence of 2016–2017 (Luzi et al., 2017), which began with the earthquake of Amatrice (M_w 6.0) in August, followed immediately after by the earthquake of Norcia (M_w 6.5) in October, the 2009 L'Aquila (M_w 6.1) seismic episode that lasted about 1 year (Chiaraluce et al., 2011; Valoroso et al., 2013) and the 1997 Umbria–Marche sequence that started with a *ML* 4.5 foreshock 23 days before the main events having M_w 5.5 and M_w 6.0 (Castro et al., 2002). Because of the high seismic risk that these earthquakes impose in the region, it is important to understand how the seismic waves attenuate with distance. Several studies have already been conducted in this region to investigate the properties of seismic wave attenuation, especially after the occurrence of significant earthquakes that have made new data available. For instance, Bindi et al. (2009) and Malagnini et al. (2011) analyzed foreshocks and aftershocks of the 2009 L'Aquila earthquake (central Italy) and used a coda-normalization technique to obtain ground-motion prediction relations valid for this region. De Lorenzo et al. (2013) determined the attenuation properties of coda waves using data from a temporal array deployed during the 1997 Umbria–Marche earthquake sequence to estimate the quality factor Q for both P and S waves. They found that $Q_P/Q_S > 1$ and concluded that the rocks in the Umbria–Marche region are partially saturated with a heterogeneous degree of fluid. Other previous attenuation studies in this region have been made by Del Pezzo and Zollo (1984) using data from the *Ms* 5.8 Norcia earthquake that occurred in the Umbria region in September 1979. They estimated coda Q and the turbidity coefficient and concluded that scattering losses are the main cause of S-wave attenuation. Castro et al. (1999, 2004) and Bindi et al. (2004) studied S-wave attenuation with seismic records from the 1997 to 1998 Umbria–Marche sequence. Castro et al. (1999) determined empirical attenuation functions for P and S waves and studied Q anisotropy. They found that for deep wave paths and low frequencies ($f < 4$ Hz), $Q_{SV} > Q_{SH}$. Castro et al. (2004) and Bindi et al. (2004) found that at high frequencies ($f > 8$–10 Hz), the frequency dependence of Q weakens, taking a value between 318 and 438. Most recently, Pisconti et al. (2015) used data from permanent and temporal stations deployed during the same 1997 seismic sequence to estimate intrinsic and scattering Q using multiple lapse time window analysis. They concluded that the crustal heterogeneities that produce seismic scattering in central Italy are important at low frequencies ($f < 2$ Hz). All these previous studies of attenuation provide average estimates of Q for different frequencies but do not account for the variability of Q with depth. These average values of Q are typically representative of large, sampled volumes that include the crust and part of the upper mantle. To estimate ground motion intensity of specific paths, it is important to use the average value Q along the specific path instead of regional averages. This is particularly important for shallow earthquakes that radiate seismic waves when travelling along the near-surface parts of the crust and that tend to have both low Q and low shear-wave velocity values. For these reasons, it is important to use a depth-dependent attenuation model.

Although previous results are difficult to compare because they are based on data sets that sample different crustal volumes, a common feature in central Italy is the significant attenuation of seismic waves, especially at high frequency, compared to other regions of Italy (i.e. Castro et al., 1999; Luzi et al., 2017). The spectral inversion studies have generally provided complex parametric descriptions for geometric spreading (Bindi et al., 2004; Malagnini et al., 2011; Pacor et al., 2016), while for anelastic attenuation, the frequency dependence of Q remains a consistent feature (Ameri et al., 2011; Bindi et al., 2017). However, the depth dependence of Q has not been considered, and the quality Q obtained by previous studies is an average value of the crustal volume investigated.

Estimates of Q are also important to determine source parameters, such as the stress drop, and to evaluate earthquake damage-related radiation due to changes of rock properties (Ben-Zion & Ampuero, 2009; Castro & Ben-Zion, 2013). In a recent study of ground motion prediction in the L'Aquila region, Pacor et al. (2016) observed that earthquake depth seems to control the stress drop scaling. In this case, source parameters were obtained using empirically determined nonparametric attenuation functions to infer the stress drops.

In this paper, we characterize the quality factor Q of shear waves (Q_S) with depth using a large collection of seismograms recorded since 2008 by the National Accelerometric Network (RAN, *Rete Accelerometrica Nazionale*), the National Seismic Network (RSN, *Rete Sismica Nazionale*) and other temporal stations that operated in central Italy during main seismic sequences. We determine a frequency-dependent 1D Q_S model of the crust that is compatible with the velocity model obtained for central Italy by De Luca et al. (2009) which is also used to locate the earthquakes in that region. The Q_S model consists of three layers over a half-space, obtained following the two-step inversion scheme proposed by Castro et al. (2019). The resulting depth-dependent Q model indicates that S waves attenuate significantly more when traveling along the 4 km-thick near-surface layer. Finally, we obtain Q-frequency relations, for each layer of the model, that can facilitate the Q correction of ground-motion records.

2. Data

The data set used in this study consists of 1029 earthquakes located in the central region of Italy (Fig. 1) and recorded by 414 local stations. This data set is composed of acceleration and velocity earthquake signals, recorded since 2008 and includes data mainly from the 2009 L'Aquila (M_w 6.1) sequence, already analyzed by Pacor et al. (2016), and the 2016–2017 central Italy (M_w 6.5) sequence. Figure 2 shows the depth, magnitude and hypocentral distance distribution of the records. Most of the events analyzed have focal depths between 8 and 10 km and a magnitude of 3.1. The number of events decreases as the magnitude increases, as predicted by the Gutenberg–Richter law. The maximum local magnitude of the events is 6.3 (2016 Norcia earthquake), and there is a gap of earthquakes between 4.9 and 5.2 and between 5.6 and 5.9. Most earthquakes in the data set are local events (hypocentral distance less than 100 km), and very few events have hypocentral distance greater than 150 km. The stations belong to the following permanent networks operated by the *Istituto Nazionale di Geofisica e Vulcanologia* (INGV), the National Seismic Network (RSN) and the Mediterrean Network (Mednet). The rapid response networks are operated together with the University of Genova and the *Reseau Seismologique and Geodesique Francais* (RESIF). Other permanent stations belong to the National Accelerometric Network (RAN) operated by the Department of Civil Protection. Stations from temporal networks were also used, and those include the networks for aftershock monitoring (Margheriti, 2011), for site effects (Bergamaschi, 2011; Cultrera et al., 2016) and for seismic microzonation (Working Group SM-AQ, 2010; Cara et al., 2019). The acceleration records can be obtained from the Italian Accelerometric Archive (http://itaca.mi.ingv.it), and the velocity records from the European Integrated Data Archive (EIDA; http://eida.rm.ingv.it).

Fig. 1

Maps of central Italy showing the location of earthquakes (circles), stations (triangles) used and

source-station paths

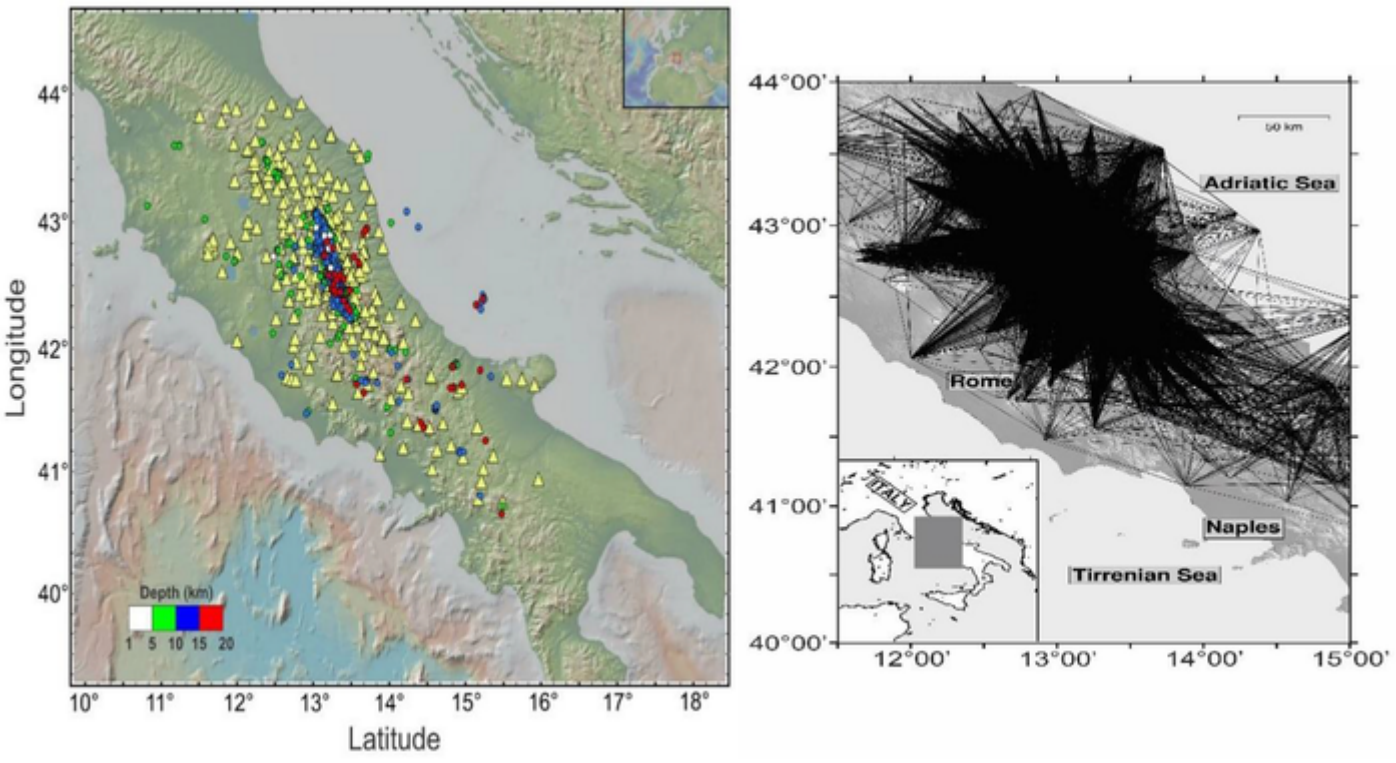

Fig. 2

Number of events analyzed: **a** focal depth distribution; **b** magnitude distribution; **c** hypocentral distance distribution

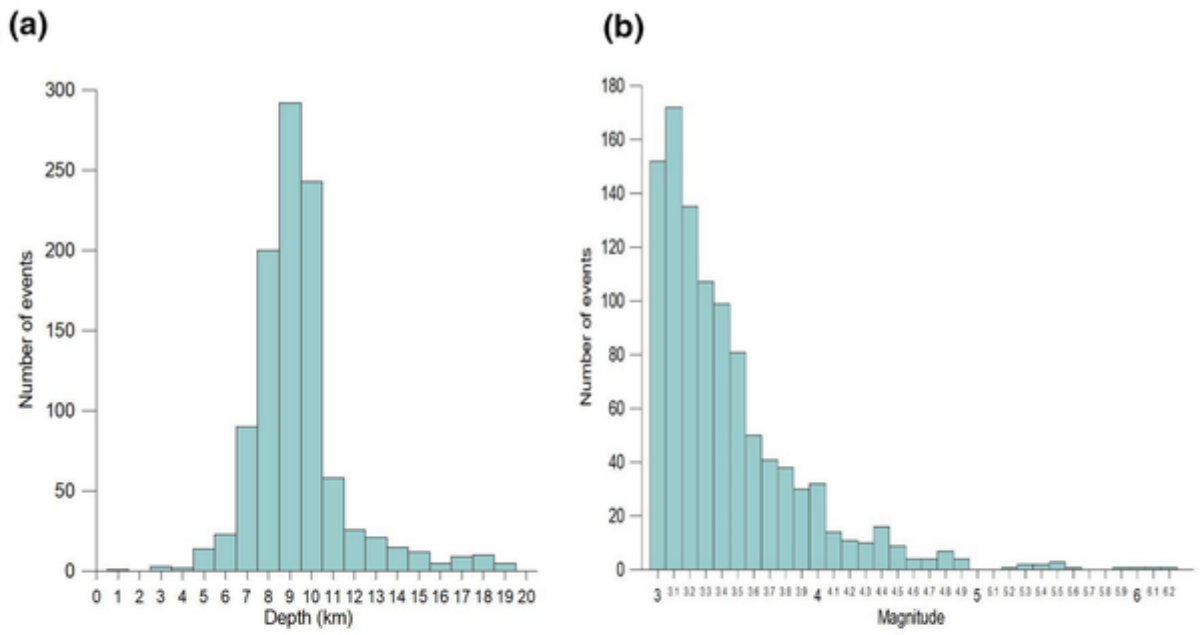

The collection of records selected for this study is composed of 63,459 signals in the local magnitude range of 3–6.3 with hypocenter distances of less than 155 km for the analysis. Figure 1 (right) shows the ray-path coverage of the data set selected, showing a dense coverage in the central zone of the investigated region. We limited the analysis to this 155 km regional hypocentral distance because there are less recordings beyond this distance (Fig. 2) and to include only source-station paths that sample the crust and the upper mantle. We also observed that the rate of amplitude decay with distance is very similar between 70 and 155 km (Fig. 3), suggesting that the geometrical spreading is about the same up to 155 km. The time windows used to calculate *S*-wave spectral amplitudes were selected using a distance-dependent energy criterion. A minimum length of 4 s was used to be able to resolve above 1 Hz for the range records with a close hypocenter distance. The time windows start 0.1 s before the direct shear wave arrival and end when the accumulated energy of the record reaches 90% of the total for hypocenter distances $r < 25$ km, 80% for $r = 25$–50 km and 70% for $r > 50$ km. These distance-dependent criteria permit to determine time windows containing *S* waves in a semiautomatic mode, avoiding surface-wave contamination. These windows are also tapered with a Hanning window, and the resulting spectral amplitudes are smoothed with the Konno and Ohmachi

spectral amplitudes to be used in the analysis: SNR = 10 for 0.2–0.4 Hz, SNR = 5 for 0.4–15 Hz and SNR = 10 for $f > 15$ Hz. More details on the data processing can be found in Pacor et al. (2016).

Fig. 3

The frame on top shows nonparametric attenuation functions for all frequencies, and the bottom plot for 0.5 Hz (black line), 1 Hz (blue), 4 Hz (red), 10 Hz (purple) and 20 Hz (green). For comparison, the dashed line is the geometrical spreading function defined in Eq. (5)

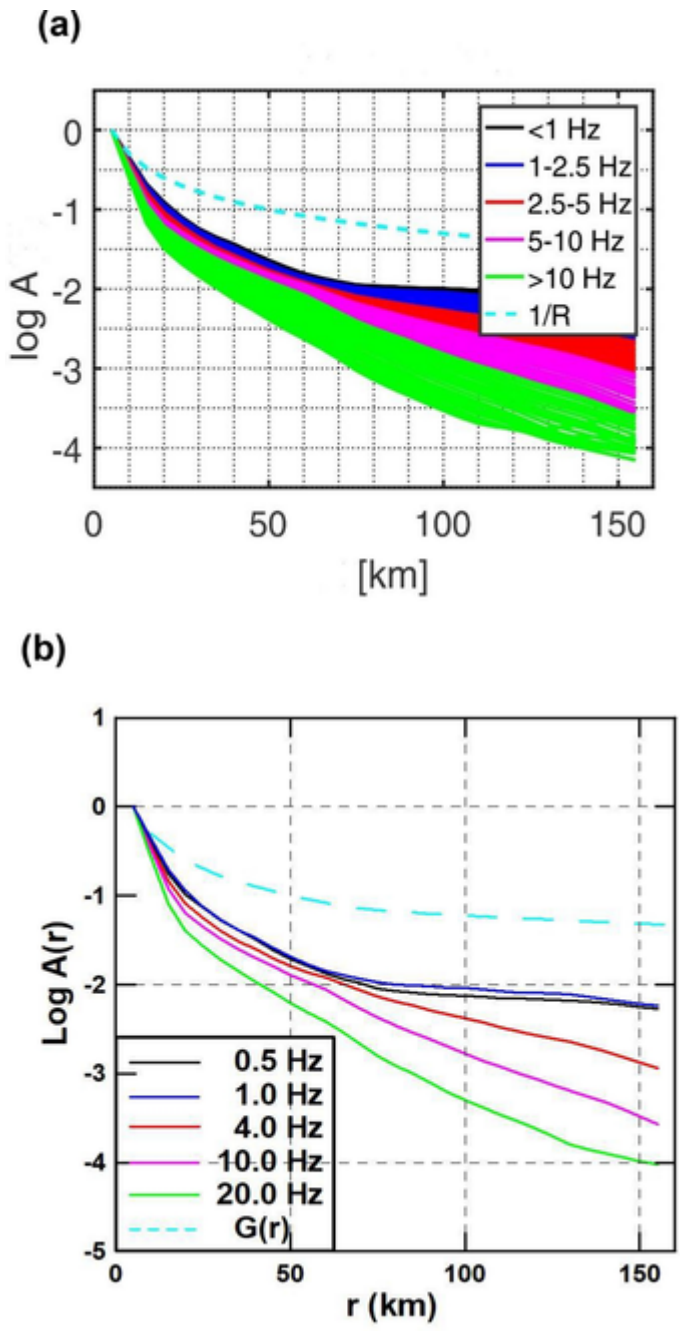

3. Method

To determine a depth-dependent shear-wave attenuation model for central Italy, we consider a 1D layered Q model, following the procedure introduced by Castro et al. (2019). In this technique, average nonparametric attenuation functions (NAF) are determined first using a linearized model. The NAF are used to separate source and site effects by correcting the observed spectral amplitudes for attenuation effects. In this approach, the residuals between the scaled NAF and the observations are interpreted as site effects.

In this paper, we determined simultaneously source, site and nonparametric attenuation functions with a generalized inversion, as in Oth et al. (2011) and Pacor et al. (2016). The advantage of this technique is that only one inversion for each frequency is required to retrieve source and path effects. Then, specific source-station attenuation paths are used with an attenuation parametric model to estimates values of Q at different depths.

A general representation of the observed spectra $U_{ij}(f,r_{ij})$ for a fixed frequency f from a source $S_i(f)$ recorded at the j site can be expressed as:

$$U_{ij}(f,r_{ij}) = S_i(f)\,A(f,r_{ij})Z_j(f) \quad (1)$$

where $Z_j(f)$ represents the site effects, and $A(f,r_{ij})$ is the nonparametric attenuation function (NAF) that accounts for energy loss due to intrinsic and scattering attenuation and to geometrical spreading.

We used a two-step technique to estimate the crustal structure of Q. We first inverted Eq. (1) to retrieve the average NAF for each frequency to characterize the spectral amplitude decay with distance r.

Because the good coverage of the data set (Fig. 1), in terms of number of events and azimuthal distribution of stations, Eq. (1) can be solved following a nonparametric approach (e.g. Castro et al., 1990, 1996; Oth et al., 2008; Parolai et al., 2000) in a single step as in Oth et al. (2011). The unresolved degree of freedom between site and source terms is eliminated by fixing the site amplification of a reference site to one. To select the reference station, a preliminary inversion was computed using the vertical components of the spectral amplitudes and fixing the average site effect of all sites to one. Horizontal-to-vertical spectral ratios (HVSR) were also calculated to estimate the

2.3, in the frequency band between 0.2 and 30 Hz. The resulting reference stations are SLO, LSS, T1217 and T1221. These sites were also identified by Priolo et al. (2019) as possible reference sites by decomposing the residuals of response spectra and evaluating the site effect contribution. The inversion is also constrained normalizing the spectral amplitudes at 5 km by making $A(f,5) = 1$ at all frequencies. A smoothing constraint is included when inverting Eq. (1), making the NAF monotonically decreasing functions of distance. The resulting attenuation functions implicitly contain the effects of geometrical spreading and total Q.

We corrected the observed spectral amplitudes for attenuation effects using the NAF. Then, the corrected amplitudes can be written as:

$$D_{ij}(f) = S_i(f)\, Z_j(f) \tag{2}$$

Since we are interested in specific source-station attenuation paths, we can eliminate source and site effects calculating the following ratio:

$$\frac{U_{ij}(f, r_{ij})}{D_{ij}(f)} = A_{ij}^{p}(f, r_{ij}) \tag{3}$$

where $A_{ij}^{p}(f, r_{ij})$ represents the attenuation between the source i and the recording site j. This function is parameterized as:

$$A_{ij}^{p}(f, r_{ij}) = G_{ij}(r_{ij}) \exp\left[\frac{-\pi f r_{ij}}{Qs\beta}\right] \tag{4}$$

where $G_{ij}(r_{ij})$ is the geometrical spreading function, and Qs and β are the shear-wave quality factor and velocity, respectively.

In this study, we assume the following geometrical spreading function:

$$G(r) = \begin{cases} 5/r & 5 < r < 70 \\ 5/\sqrt{70r} & r \geq 70 \end{cases} \tag{5}$$

Equation (5) is an approximation of the function estimated by Pacor et al. (2016) for the L'Aquila region, a subdomain of central Italy. Equation (5) normalizes the amplitudes at the minimum distance of 5 km and changes the rate of amplitude decay at 70 km, where the NAF also show a change on amplitude decay (Fig. 3). The change of rate of amplitude decay at $r > 70$ km may be due to the enrichment of the spectral amplitudes due to refracted and surface waves that may have contaminated the time windows used to calculate the direct S-wave spectral amplitudes.

The second step of the inversion consists of finding discrete values of Qs for a layered-space fixing f. As in Castro et al. (2019), Eq. (4) can be expressed as:

$$M_{ij} = C \sum_{k=1}^{N} \frac{r_{ijk}}{\beta_k Q s_k} \tag{6}$$

where M_{ij} is the logarithm of the observed amplitude corrected for source, site and geometrical spreading effects, for a given frequency f. $N = 4$ is the number of layers of the model, k refers to the layer and $C = -\pi f \mathrm{Log}(e)$. We calculate r_{ijk} by ray trace using the standard velocity model of central Italy (Chiaraluce et al., 2011; De Luca et al., 2009; Valoroso et al., 2013) listed in Table 1.

Table 1

Velocity model used to calculate ray travel times

Depth (km)	Vp (km/s)	Vs (km/s)	Thickness (km)
0.0	5.0	2.70	4.0
4.0	6.2	3.35	6.0
10.0	6.3	3.41	15.0
25.0	7.0	3.78	5.0
30.0	8.0	4.32	100.0

4. Results

Figure 3 shows the nonparametric functions (NAF) obtained for all the frequencies analyzed and for the five frequencies selected from 0.5

increment of 5 km. The rate of amplitude decay with distance changes gradually with frequency (Fig. 3a); for instance, for $f < 1$ Hz, the amplitude decay of the NAF is approximately the same within that frequency range. However, at high frequencies ($f > 10$ Hz), the NAF attenuate more than those at low frequencies ($f < 1$ Hz). The changes of rate of amplitude decay with distance can be due to geometrical spreading being affected by the complex crustal structure of central Italy, particularly at shallow depths. For instance, Pacor et al. (2016) found that in this region, the geometrical spreading function $G(r)$ that better describes the observed amplitude decay is $G(r) \sim 1/r$ for $r < 10$ km, $G(r) \sim r^{-1.68}$ for 10–70 km and $G(r) \sim r^{-0.64}$ for $r > 70$ km. The NAF (Fig. 3) show a change of rate of amplitude decay for $r < 10$ km and another near 70 km, particularly at low frequencies ($f < 1$ Hz). To be consistent with previous studies, we define the geometrical spreading as in Eq. (5) to correct the observed amplitudes.

To analyze the possible radial variability of the attenuation, we selected an M 4.3 earthquake with focal depth of 9.8 km, located in the center of the recording network (42.72 N, 13.21 E) and recorded by 148 stations. We calculated the residual between the average attenuation at 4 Hz, represented by $A(f, r_{ij})$ (Fig. 3) and the attenuation between that event and the recording sites ($A_{ij}^{p}(f, r_{ij})$). The continuous line in Fig. 4 (left) is the average NAF at 4 Hz, and the circles are the attenuation for each source-station path, which tend to be slightly above the average attenuation. The residuals, also shown in Fig. 4, do not show any radial trend. The high residual (above 0.5) of two of the 148 stations is probably related to near-site attenuation. The proximity between the observed amplitudes and the NAF suggest that the nonparametric functions capture some of the Q structure and the depth dependence of the shear-wave attenuation. Being that the case, the determination of source parameters using NAF (e.g. Pacor et al., 2016) may be a more reliable method to estimate the earthquake stress drop.

Fig. 4

The red line (left frame) represents the average attenuation at 4 Hz, and the circles the source-station attenuation (Eq. (4)). We selected an M 4.3 earthquake (event 252) with focal depth of 9.8 km which was recorded by 148 stations. The right fame shows the residual between the average NAF and the attenuation along the respective source-station path versus azimuth

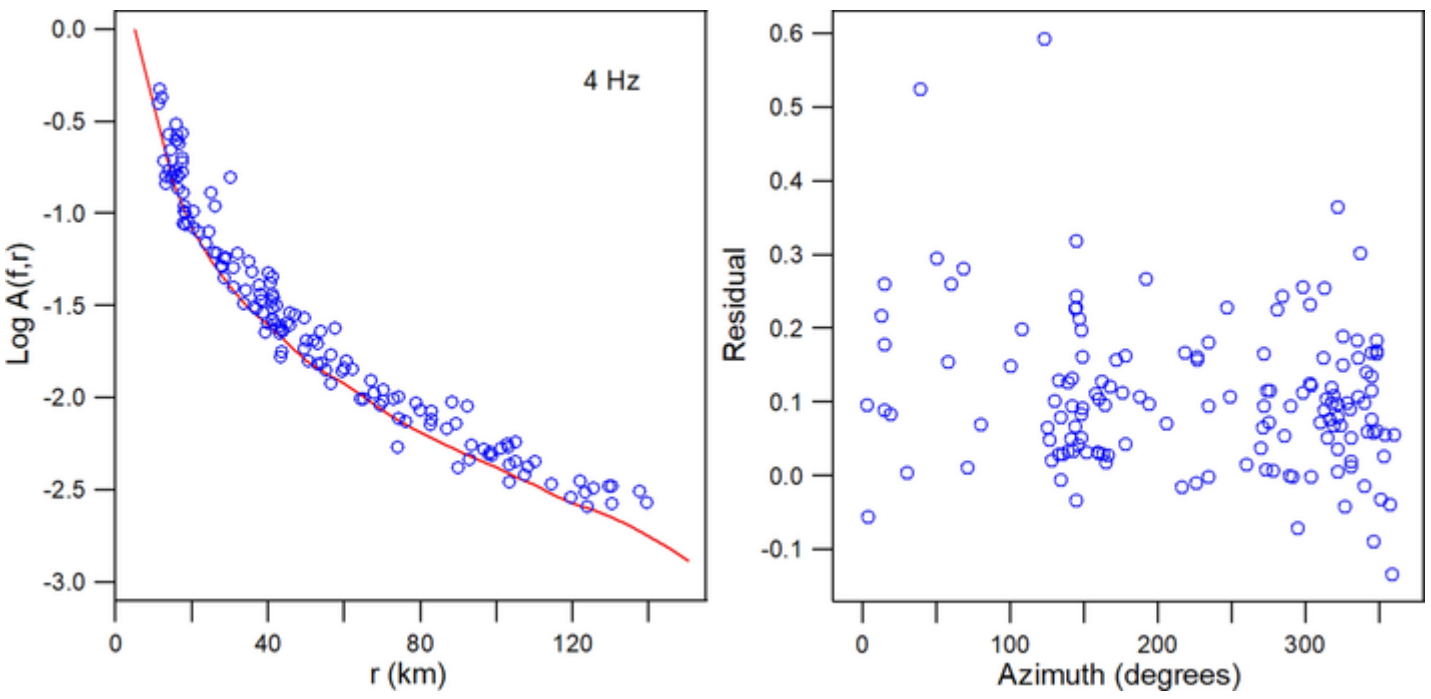

We calculate separate inversions using Eq. (6) for five visually chosen central frequencies (0.5, 1.0, 4.0, 10.0 and 20 Hz) based on the frequency band of the data analyzed. Since the NAF (Fig. 3a) show a gradual change of rate of amplitude decay with distance within well-defined frequency bands, we consider those five frequencies representative of low-, intermediate- and high-frequency bands, and we used only those (Fig. 3b) for further analysis. Figure 5 shows the estimates of $1/Q_S$ and Q_S versus the layer depth for the five frequencies considered. In general, Q_S increases with frequency and with depth, although between 4 and 15 km, Q_S is approximately constant for a given frequency. The depth-dependent Q_S model obtained (Fig. 5) shows that shear waves will attenuate considerably more when traveling along the last 4 km of the near-surface layer, particularly at low frequencies. In this layer, Q_S varies between 2.1 at 0.5 Hz and 152 at 20 Hz. It is interesting to note that at high frequencies ($f \geq 10$ Hz), Q_S converges to a value between 151 and 152. At larger depths (4–10 km), Q_S takes values between 26 at 0.5 Hz and 632 at 20 Hz. Between 10 and 15 km depth, Q_S is approximately the same as in the previous layer. We cannot estimate Q_S at deeper layers because most earthquakes in central Italy are shallow events with focal depths less than 18 km.

Fig. 5

Values of Q and $1/Q$ versus mid-depth (H) of the layer in km, for the five frequencies analyzed (0.5, 1, 4, 10 and 20 Hz), resulting from the inversion. Red circles are for 0.5 Hz, gray diamonds for 1 Hz, blue circles for 4 Hz, green circles for 10 Hz and red diamonds for 20 Hz

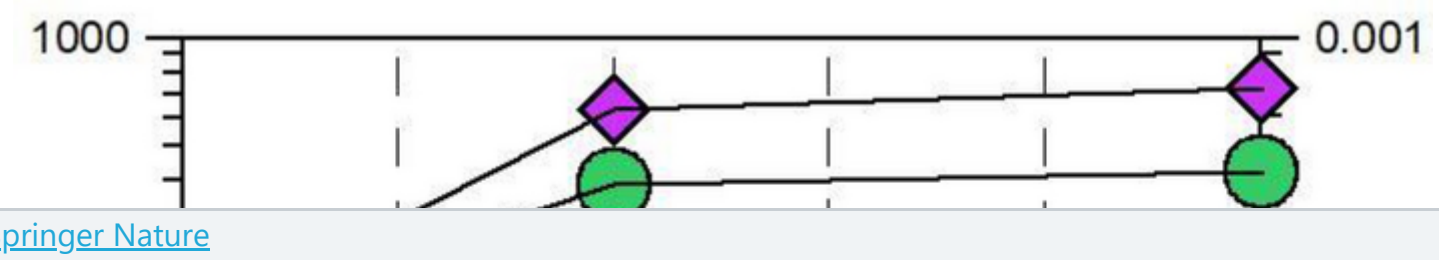

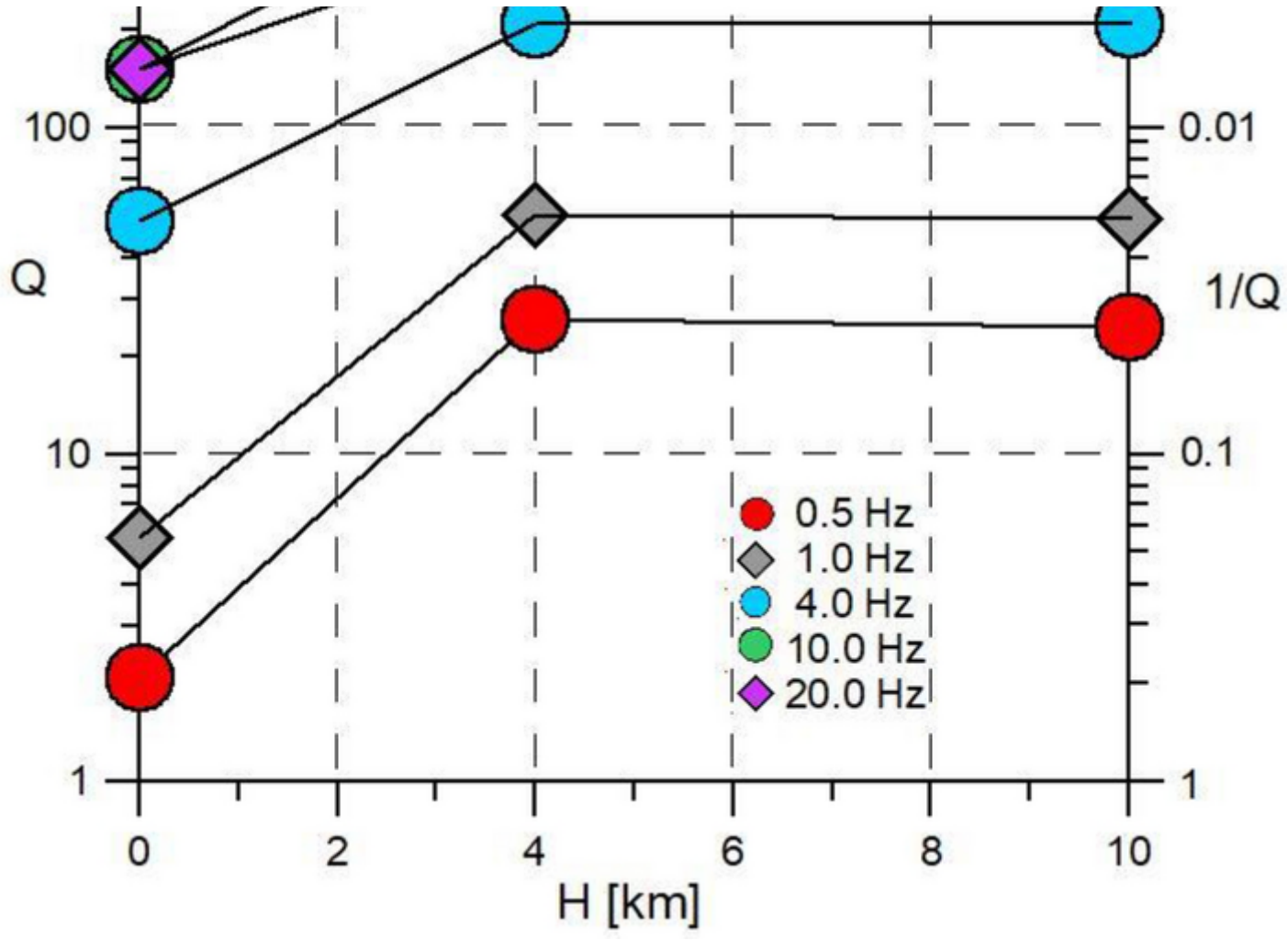

Figure 6 shows the values of Q_S obtained as a function frequency for each layer of the model and the error associated to the estimates. The root mean square (RMS) is also shown (left bottom frame). The RMS values range between 0.59 and 0.84 for the different frequencies. These low values of the residual mean are low enough to validate our results. The errors in the estimates of *1/Q* vary between 0.56 and 1.97%, and we propagated them to the Q_S values in Fig. 6. It is interesting to note that in the first layer (depth less than 4 km), Q_S flattens to a constant value of 151.5 at $f > 10$ Hz. Castro et al. (2000, 2002, 2004) found in central Italy that for $f > 10$ Hz, the frequency dependence of Q weakens. Castro et al. (2004) estimated that for $f > 10$ Hz, the average $\tilde{Q}$ has an approximately constant value of 438. In the same region, Bindi et al. (2004) found that $\tilde{Q} = 318$ for $f > 8$ Hz and hypocenter distances $r < 60$ km. Since most of the earthquakes analyzed have focal depths of less than 10 km (Fig. 2), it is reasonable to calculate an average Q_S from the 1D model using only the first two layers. Thus, we calculate $\tilde{Q} = 294$ at 10 Hz and $\tilde{Q} = 440$ at 20 Hz, and a mean value of 367 between 10 and 20 Hz, in coherence with the previous studies.

Fig. 6

Values of Q obtained, and error bars, as a function of frequency for the three layers of the model. The left lower frame displays the RMS of the residual mean

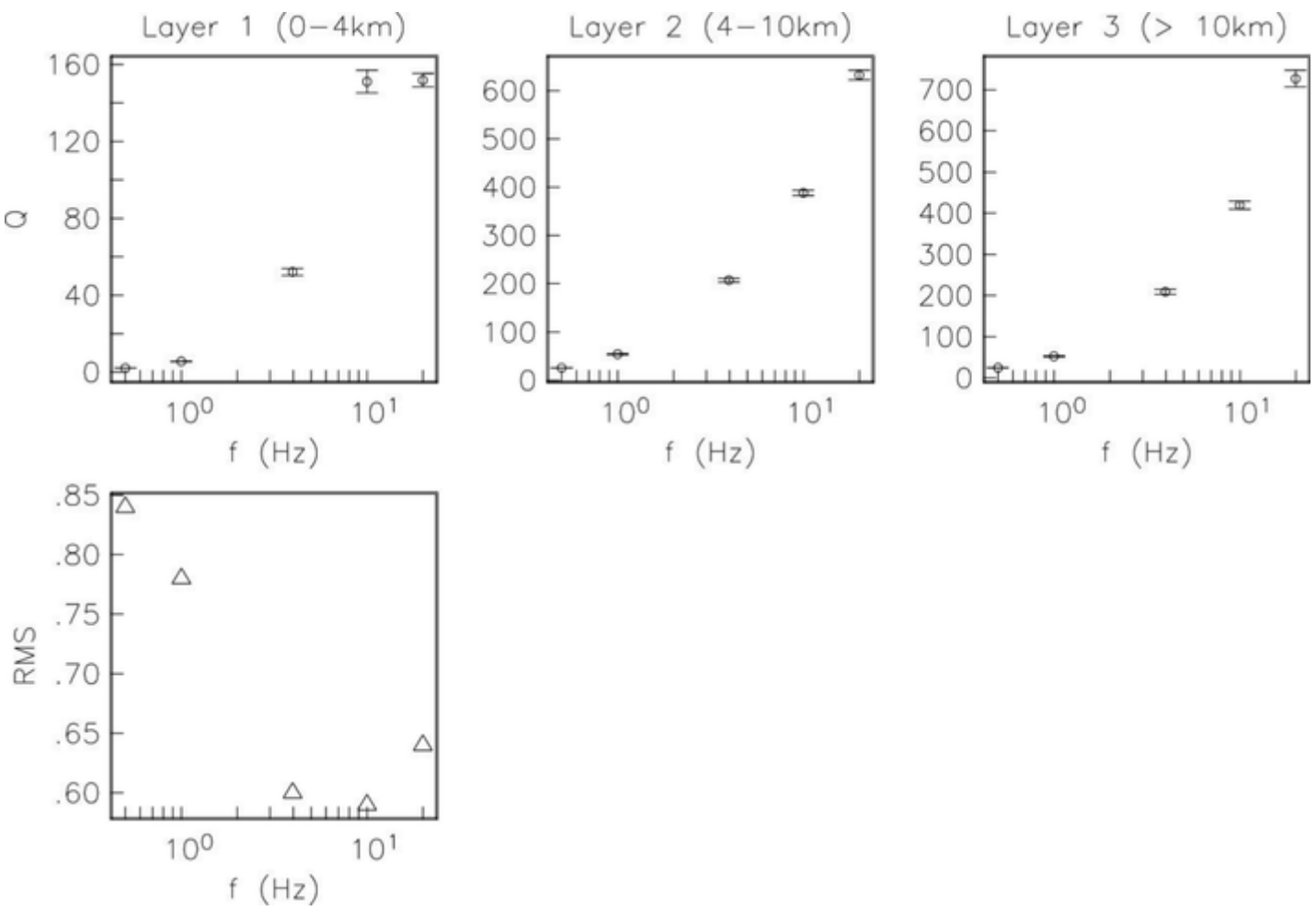

To compare these estimates of Q_S with previous attenuation studies that report average values of Q_S, we calculate for each frequency the average Q_S weighting the values of Q_S estimated according to the respective thickness using the first three layers of the 1D model (Table 1). Figure 7 displays with triangles these average values and the *Q*-frequency relation obtained by weighting in the regression the values of

is:

Fig. 7

Average crustal shear wave Q obtained using estimated Q from the three layers of the model (triangles). The circles are estimates of Q ($Q(f) = 49f^{0.9}$, $0.5 \leq f \leq 8.0$ *Hz*) reported by Bindi et al. (2004) using data from the 1997–1998 Umbria–Marche (central Italy) sequence. The diamonds are estimates of total Q from Pisconti et al. (2015). The dashed lines are the upper and lower limits expected from the estimated errors of the Q-frequency relation displayed on top of the figure (Eq. (7) in the text). The star at 20 Hz is the average from the first two layers of the 1D model ($\tilde{Q} = 367$)

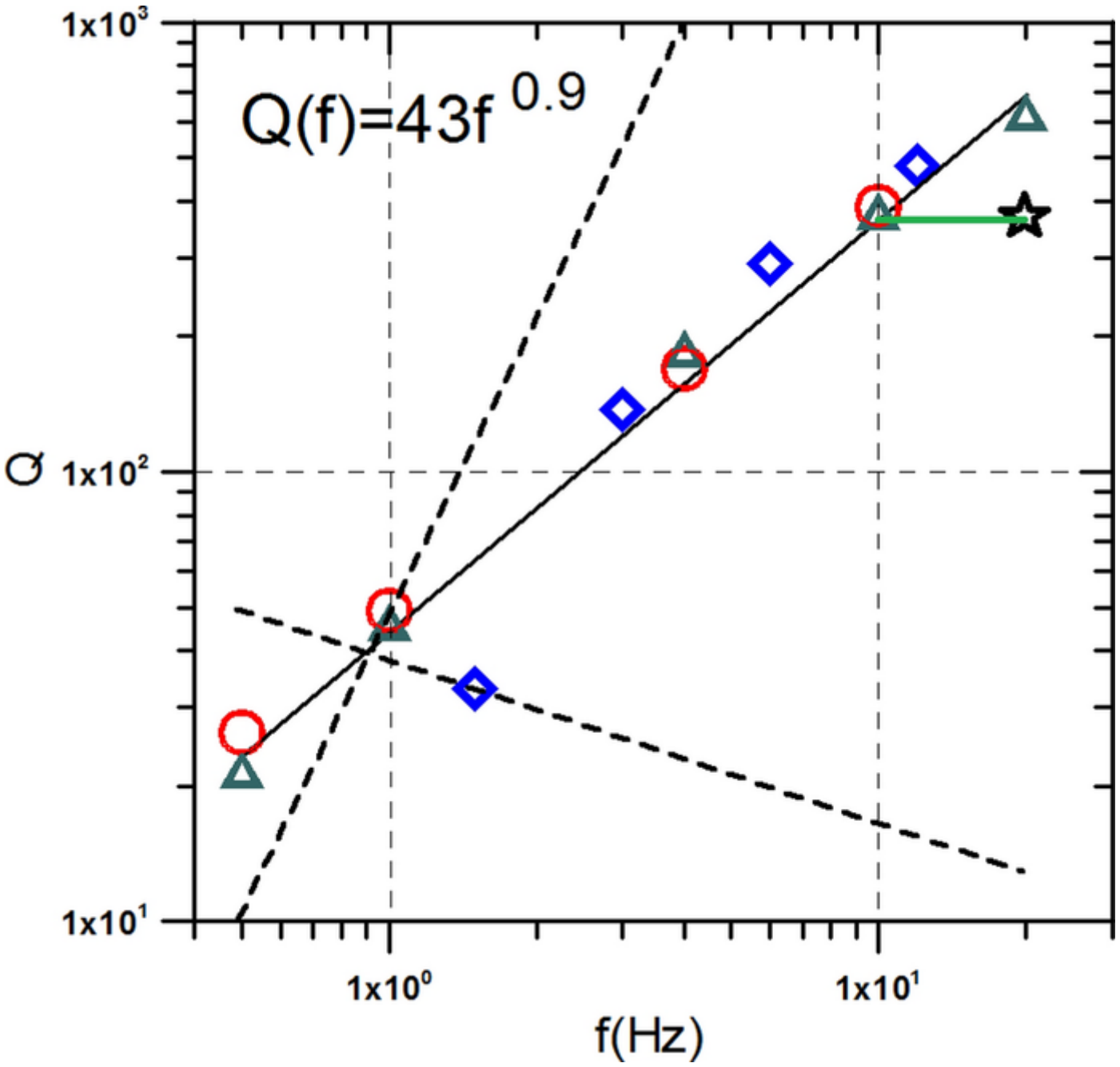

$$Q_S(f) = (42.8 \pm 5.4) f^{0.94 \pm 1.274} \quad (7)$$

For comparison, the circles show the values of shear wave Q calculated with the relation $Q(f) = 49f^{0.9}$ obtained by Bindi et al. (2004) using records from the 1997–1998 Umbria–Marche (central Italy) sequence. The diamonds in Fig. 7 are the values of total Q reported by Pisconti et al. (2015) for the same region. The dashed lines are the upper and lower limits expected from the estimated errors of the Q-frequency relation (Eq. 7).

To be able to correct the ground-motion records for attenuation, using the 1D model obtained (Fig. 5), we calculated the following Q-frequency relations by calculating a linear fit of Q versus f in the logarithm domain, weighting the values of Q with their respective standard deviation:

$$Qs(f) = (6.0 \pm 1.3)\, f^{1.25 \pm 0.15} \quad for\ h < 4\ km \quad (8)$$

where h is the depth. For the second and third layer of the model, we found:

$$Qs(f) = (52.4 \pm 1.1) f^{0.87 \pm 0.04} \quad for\ 4 < h < 10\ km \quad (9)$$

(10)

5. Discussion

5.1. Q_S and the Spectral Decay Parameter Kappa

The low values of Q_S for the first 4 km of the model can be compared with estimates of the high-frequency spectral decay parameter kappa (κ) introduced by Anderson and Hough (1984). If we consider a surface layer with low shear-wave velocity and Q underlain by a basement with higher wave-propagation velocity and Q, κ can be related to the quality factor, following Hough et al. (1988), by:

$$\kappa \sim \frac{H}{Q_1 \beta_1} + \frac{r}{Q_2 \beta_2} \tag{11}$$

where H is the thickness of the low-Q layer, and β_1 and β_2 are S-wave velocities of the near-surface layer and the basement, respectively. In this model, κ accounts for the attenuation along the path, and the near-surface parameter (κ_0) is neglected (there is no site effect).

We calculated κ using the method proposed by Anderson and Hough (1984) selecting a hard-rock station, since we determined the values of Q_S of our 1D model using site amplification-corrected spectra. The logarithm of the high-frequency S-wave spectral acceleration amplitude is least-squares fitted. κ is calculated from the slope of the linear fit which equals $-\pi \mathrm{Log}(e)\kappa$. We used records from Leonessa station (IT.LLS), one of the reference sites selected in the inversion scheme. The average frequency band used for evaluating κ is 15–30 Hz, although it varies from record to record, depending on the magnitude and distance. We estimated the high-frequency decay parameter using the rock station LSS to have an independent estimate of Q at the surface layer and to verify that the estimates of Q from the 1D model and those from κ agree.

This procedure was applied for 50 records of LLS at hypocenter distances between 15 and 57 km, and the linear least-square fit of the κ estimates gives:

$$\kappa(r) = 0.008654 + 0.0000615r \tag{12}$$

Relating Eqs. (11) and (12), $\frac{H}{Q_1 \beta_1}$ = 0.008654, and for β_1=2.7 km/s, we obtain Q_1 =171. Since κ is estimated within the high-frequency band of the spectrum, we can compare this estimate of Q with the values of our model at high frequencies. For instance, at 10 Hz, our model (Fig. 5) gives Q_S = 151, and at 20 Hz, Q_S = 152, which are comparable to the estimate of Q using the κ model. The kappa model of Anderson and Hough (1984) assumes that Q is frequency-independent, and we found from our frequency-dependent 1D Q model that at high frequencies, Q is approximately constant with frequency, in agreement with the kappa model. This has been previously observed by Castro et al. (2004) and Bindi et al. (2004) who found that at high frequencies (f > 8–10 Hz), Q in central Italy is approximately constant.

5.2. Depth-Dependent Q-Frequency Relations

Equations (8), (9) and (10) are compared in Fig. 8 which shows insignificant differences of the values of Q_S between the second (4–10 km deep) and the third layer (10–15 km deep) of the model. However, there are significant differences between the first Q_S layer and the deeper layers. At low frequency (0.5 Hz), Q_S is smaller by a factor of 12 at depths less than 4 km, and at high frequency (20 Hz), is smaller by a factor of about 3 than Q_S between 4 and 15 km depth. For depths of less than 4 km and f > 10 Hz, Q does not increase with frequency and takes a constant value of 151.5. Thus, a better representation of the frequency dependence of Q in this superficial layer is:

Fig. 8

Q-frequency relations obtained using the values of Q_S (triangles) obtained for the first 4 km of the model (left frame). The relation $Q(f) = 52.4f^{0.87}$ was obtained with the values of Q_S (red squares) estimated for the second layer of the model (4–10 km) and the relation $Q(f) = 50.6f^{0.92}$ with the values of Q_S (blue diamonds) for the 10–15 km depth layer. The dashed lines are the upper and lower limits expected from the estimated errors of the Q-frequency relations

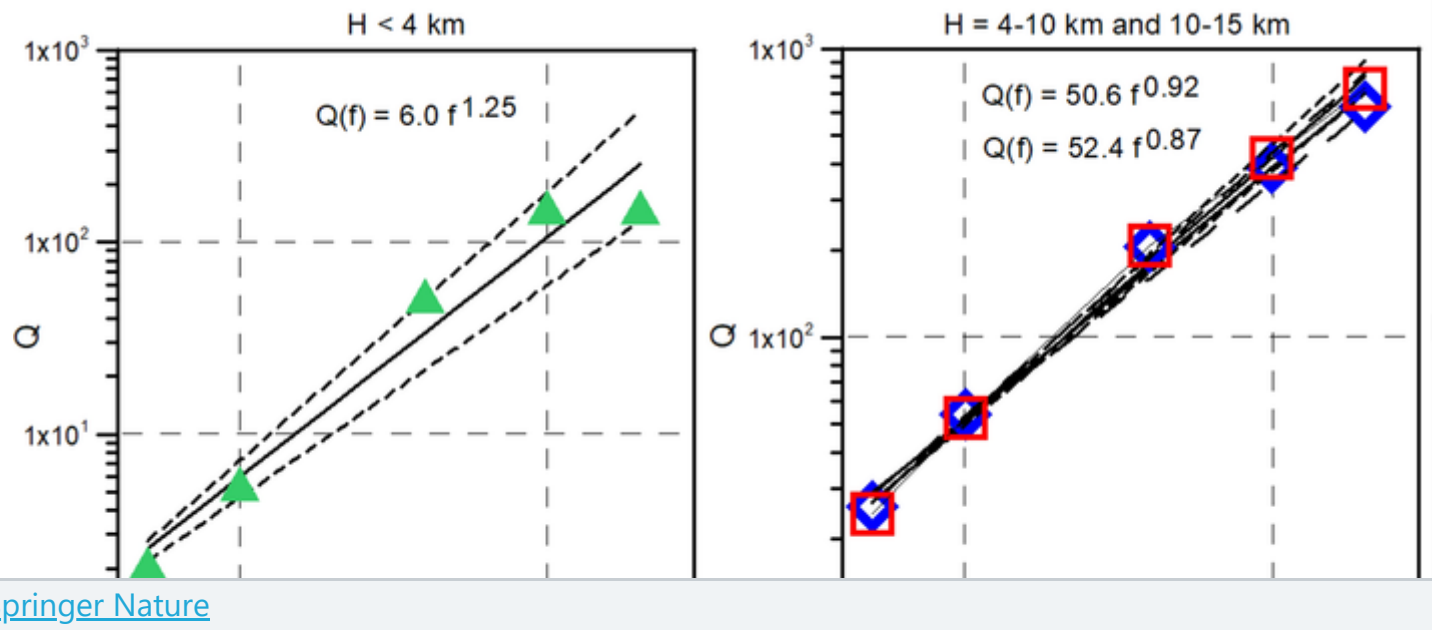

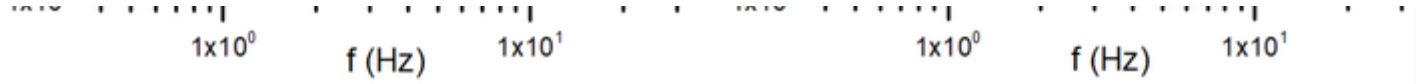

$$Q(f) = (5.5 \pm 1.1)\, f^{1.39 \pm 0.14} \quad for\ 0.5 \le f \le 10\ Hz \tag{13}$$

$$Q = 151.5 \quad for\ f > 10\ Hz \tag{14}$$

Castro et al. (2004) suggested that the change of frequency dependence of Q at $f > 10$ Hz may be related to the presence of faults in the crust. Abercrombie (1998), for instance, observed that at seismogenic depths in California, Q shows a small increase with frequency at high frequencies ($f > 10$ Hz). However, the depth of the seismogenic zone in central Italy is probably between 7 and 11 km, the depths where most events seem to occur (Fig. 2). Thus, it is more likely that the low values and weak dependence of Q_S with frequency in the first near-surface layer (depths less than 4 km) are related to the presence of sediments on top of fractured rocks in the valleys of central Italy. For instance, in the Colfiorito basin, Sano et al. (1998) reported the presence of lake deposits 35 km thick. The presence of sediments associated with low Q values in a basin is common in many other regions. In the Imperial Valley, California, Singh et al. (1982) found that in the upper 4 km, that are composed essentially of sediments, shear-wave Q_S varies between 57 and 100, and along the active Imperial fault, $Q_S = 20\,f$ ($25 < f < 3$ Hz). Rock damage generated by faulting during earthquake activity may also be the cause of low Q values. Castro and Ben-Zion (2013) found a significant variation of Q (by a factor of 3) before and after the El Mayor–Cucapah earthquake (M_w 7.2), Baja California, as a result of rock damage generated by the fault rupture. In central Italy, earthquake-generated surface damage was observed after the 24 August 2016 M_w 6.0 Amatrice event (Bonini et al., 2019). In the same region, the Norcia M_w 6.5 earthquake on 30 October 2016 also caused important near-surface ruptures (Civico et al., 2018). During this seismic sequence, shallow earthquakes, with focal depths less than 5 km, occurred before and after the main event (Chiaraluce et al., 2017).

5.3. Comparison with Previous Studies

To analyze how Eqs. (8) to (10) fit the observed NAF at different frequencies and how they compare with previous models proposed by other authors, we compare in Fig. 9 the amplitude decay with distance expected from these Q-frequency relations. The purpose of this comparison is to validate those equations for future use. Figure 9 also shows other attenuation models reported in previous studies (Bindi et al., 2009 (BND09); Malagnini et al., 2011 (MAL11); Pacor et al., 2016 (PAC16)) and the attenuation functions obtained combining Eqs. (8) to (10) with the geometrical spreading function defined in Eq. (5). Figure 9 shows the spectral amplitudes versus hypocentral distance at 0.9 Hz (top), 5.3 Hz (middle) and 15.8 Hz (bottom). The functions labeled H1 (red continuous line), H2 (red dashed line) and H3 (red dotted line) correspond to Eqs. (8), (9) and (10), respectively, and the triangles the attenuation functions calculated with the average Q_S (Eqs. (5) and (7)). For comparison purposes AQ3 it is assumed that either the whole ray path is along the first layer of the 1D model (model H1), that the seismic rays travel along the second layer, between 5 and 10 km depth (model H2), or for model H3 that the rays travel along the 10–15 km depth layer. For shallow ray paths (depths less than 4 km), the first low-Q layer (H1 model) predicts a more rapid decay of amplitudes with distance than the other models. Models H2 and H3 predict practically the same amplitude decay with distance for the three frequencies considered. For $f = 0.9$ Hz, the H2 and H3 models predict less attenuation than the observed NAF for hypocenter distances less than 100 km, but the average attenuation (triangles) follows the observed attenuation closely for $R < 80$ km. One possible explanation for this feature is that the NAF represent the average attenuation from source-station paths traveling along different crustal depths, and the 1D models H2 and H3 do not account for the contribution of the superficial layer to the total attenuation. At 0.9 Hz, model MAL11 predicts less attenuation than the other models, and the PAC16 model gives amplitude values closer to the observed NAF than the other models. At 5.3 Hz, model MAL11 is like H2 and H3 models, and the three models underestimate the observed attenuation by a factor between 1.14 and 2.21 in the 10–155 km distance range. However, the average attenuation (triangles) follows the observed attenuation better than all the other models. Models BND09 and PAC16 are similar up to 70 km. Beyond 70 km, BND09 overestimates the attenuation between a factor of 1.13 and 4.0, and PAC16 follows the observed NAF closer. At 15.8 Hz, models H2 and H3 underestimate the attenuation by a factor between 1.5 and 30 because they do not consider the low Q value of the first layer of the 1D model. The average attenuation function (triangles) follows the trend of model H3 and does not fit the observed attenuation (blue line) because at high frequencies ($f > 10$ Hz), Q is approximately independent of frequency (Bindi et al., 2004; Castro et al., 2004) and Eq. (7) is a linear fit of the three-layer average Q. At high frequencies ($f > 10$ Hz), and at 15.8 Hz, a constant $\tilde{Q} = 367$ (as in Fig. 7) fits the observed attenuation better. The bottom frame in Fig. 9 shows with stars the attenuation function calculated with Eq. (5) and a constant $Q = 367$. The other models follow the observed NAF up to about 50 km and all tend to overestimate the attenuation by a factor between 1.1 and 25.6. Model H1 overestimates the amplitude decay above 40 km because the effects of layers 2 and 3 are not considered. At low frequency (e.g. 0.9 Hz), the wave lengths are longer, the waves penetrate deeper and layers 2 and 3 have stronger effect on the amplitude decay, while at high frequencies (15.8 Hz), short-wavelength waves are more affected by the near-surface Q value of the first layer of the 1D model. The main causes of the differences between our 1D model results and those reported by other authors include: the different crustal volume sampled by the different data sets, which can impact the average value of Q obtained; and the different geometrical spreading functions adopted by other authors. For instance, at 0.9 Hz and $r < 10$ km, all the attenuation curves, except for H1, are similar because the geometrical spreading used is approximately the same ($G(r) \sim 1/r$). The attenuation function calculated with model H1 is different because Q is lower than that used for the other models (e.g. a factor of 23 lower than the MAL11 model). For $r > 30$ km, the MAL11 model predicts less attenuation than the other models because $G(r) \sim 0.03(r/30)^{-0.7}$, while BND09, for AQ4 instance, uses $G(r) = 8.5/r$.

Comparison of observed NAF (blue lines) with hypocentral distance at 0.9 Hz (top), 5.3 Hz (middle) and 15.8 Hz (bottom) with different attenuation models: light gray lines from Bindi et al. (2009), gray from Malagnini et al. (2011) and black from Pacor et al. (2016). The red continuous lines are the amplitude values calculated with Eq. (8), the dashed lines with Eq. (9) and the dotted lines with Eq. (10) that correspond to Q in the first ($h < 4$ km), second (4–10 km) and third layer (5–15 km) of our model, respectively. The triangles are the average attenuation calculated with Eqs. (5) and (7), and the stars are the average attenuation for the 15.8 Hz (bottom frame) attenuation function calculated with a constant $Q = 367$ and Eq. (5)

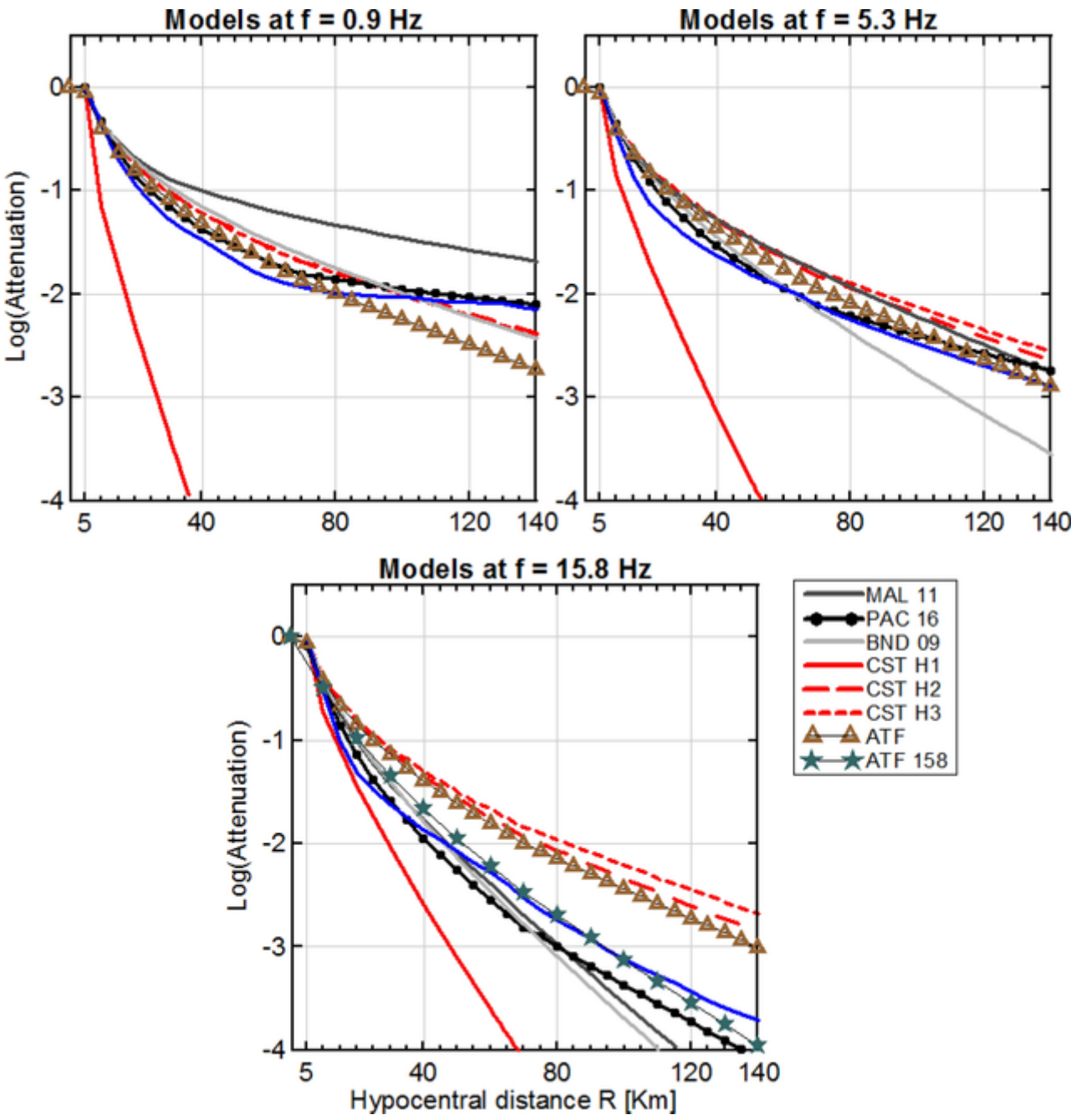

5.4. Effects of the Depth-Dependent Q on Source Spectra

To illustrate the effects of the depth-dependent Q model on the spectral amplitudes, we can compare it with the theoretical attenuation resulting from a uniform Q model:

$$A_t(f,r) = A_0 \dot{e}^{-\pi f r/Qv} \quad (15)$$

We assume vertical incidence and make $A_0 = 1$, $r = 9$ km and average values of Q given by Eq. (7) and an average shear-wave velocity $v = 3.09$ km/s. For the 1D Q_S model, the seismic ray travels 5 km in the second layer of the model and 4 km in the low-Q layer. We use Eqs. (8) and (9) for the values of Q in the first and second layer, respectively. The S-wave velocities for the first and second layers are 2.7 km/s and 3.35 km/s, respectively. At low frequencies ($f < 4$ Hz), the depth-dependent Q model reduces the spectral amplitudes by a factor between 1.4 and 2.7, while the average model reduces the amplitudes by a factor between 1.2 and 1.3. At high frequencies (10–20 Hz), the 1D average Q model (Eqs. 8, 9) reduces the amplitudes by a factor between 1.6 and 1.7, but if we use instead Eqs. (9) and (14), the amplitudes are reduced by a factor between 1.5 and 2.1. In contrast, the average Q model (Eq. 7) reduces the amplitudes by a factor of only 1.3. Thus, we expect that at short hypocentral distances, the depth-dependent Q model will have a strong effect at low frequencies (an amplitude reduction of more than 40%) and less significant effect at high frequencies (amplitude reduction of less than 60%). This observation can explain why the corner frequency estimated for large- and moderate-size earthquakes may tend to be smaller than the actual value, as explained below.

As mentioned previously, stress drop scaling in the L'Aquila region may be controlled by earthquake focal depth (Pacor et al., 2016). Since the attenuation plays an important role in the evaluation of source parameters, we analyze the effect of the Q correction on the source spectra by calculating the source acceleration spectra predicted for a magnitude M_w 3.5 event using the ω^2 model (Brune, 1970)

vertical incidence and using and average Q value (Eq. 7) and the 1D Q model. Because of the short distances considered, the source spectra corrected with the average Q closely follow the original source function. However, when we correct the source function with the 1D Q model, the spectral amplitudes are attenuated considerably more. In the first case (at 5 km), most of the travel path is within the low-Q layer of the model, and Eq. (8) dominates the attenuation. For the 9 km hypocenter distance we used Eq. (9) for the first 5 km of the wave path and Eq. (8) for the last 4 km. At 10 Hz, for instance, the use of an average crustal Q reduces the amplitude of the source function by about 20%, while the 1D Q model reduces the spectral amplitude by 43% at the same frequency. Table 2 lists the corner frequency of the source acceleration spectra after the Q correction using the depth-dependent attenuation model and the average Q for different hypocentral distances. The stress drop ($\Delta\sigma_B$) was calculated with the Brune (1970) model using (Singh & Ordaz, 1994):

$$f_c = 0.49\beta\left(\frac{\Delta\sigma_B}{M_0}\right)^{1/3} \tag{16}$$

where f_c is the corner frequency, $\beta = 3.0$ km/s is the average shear-wave velocity and $M_0 = 2.2387 \times 10^{14}$ N-m is the seismic moment for an $M_w = 3.5$ earthquake. The corner frequency was estimated following Andrews (1986) as:

$$f_c = \frac{1}{2\pi}\sqrt{\mathrm{SV/SD}} \tag{17}$$

where

Table 2

Corner frequency and stress drop estimates using the 1D Q model and the average Q for an $M_w = 3.5$ event

Hypocentral distance (km)	Corner frequency (Hz)	Stress drop (MPa)	Model
5	3.73	3.7	1D
5	2.94	1.8	Average
9	3.67	3.5	1D
9	2.89	1.7	Average
40	6.35	18.0	1D
40	2.99	1.9	Average

$$\mathrm{SD} = 2\int_0^\infty D^2(f)\,\mathrm{d}f \tag{18}$$

$$\mathrm{SV} = 2\int_0^\infty V^2(f)\mathrm{d}f \tag{19}$$

$D(f)$ and $V(f)$ are the displacement and velocity source spectra, respectively. The corner frequency changes 21% by using the average Q instead of the 1D Q model for hypocentral distances between 5 and 9 km, for vertical incidence (epicentral distance zero). The 9 km corresponds to the focal depth where most of the events were recorded (Fig. 2), and it is within the likely depth of the seismogenic zone in central Italy (between 8 and 10 km). The stress drop remains approximately constant between 5 and 9 km depth for the same magnitude event regardless of the Q correction (Table 2). This indicates that the variations of Q have little effect on the stress drop dependence on depth.

For a hypocentral distance of 40 km and a focal depth of 9 km, the rays travel half of their path along the second layer of the model, at 3.35 km/s (Table 1), and the other half along the 2.7 km/s layer. In this case, f_c and the stress drop change 53% and 90%, respectively, when using the 1D Q model instead of the average Q. These results emphasize the importance of using the 1D Q model, particularly for events with shallow focal depth (less than 10 km) and large hypocentral distances (greater than 40 km).

6. Conclusions

We determine a depth-dependent Q_S model for S waves in central Italy, and we find that Q_S increases with frequency at depths greater than 4 km, and it has lower values at shallow depths (Fig. 6). At shallow depths ($H < 4$ km) and high frequencies ($f > 10$ Hz), Q becomes frequency-independent in this region, as reported in previous studies (Castro et al., 2000, 2002, 2004 and Bindi et al., 2004). At low frequency (0.5 Hz), Q_S is smaller by a factor of 12 at depths less than 4 km, and at high frequency (20 Hz), smaller by a factor of about 4 than Q_S between 4 and 15 km depth. The average value of Q_S is consistent with previous studies made in this region of Italy and can be

functions better. We evaluate the frequency dependence of Q_S with depth, and we find the following relations: $Q_S = 5.5f^{\quad}$ ($0.5 \leq f \leq 10$ Hz) and $Q_S = 151$ ($f > 10$ Hz) for 0–4 km; $Q_S = 52.4f^{0.87}$ ($0.5 \leq f \leq 20$ Hz) for 4–10 km; and $Q_S = 50.6f^{0.92}$ ($0.5 \leq f \leq 20$ Hz) for 10–15 km depth. The low values of Q_S in the near-surface layer are probably related to several factors: the complex crustal structure that combines shallow faults that are evidenced by earthquakes with focal depths less than 5 km (Chiaraluche et al., 2017); valleys filled with low-shear-velocity sediments, like the Colfiorito basin (Sano et al., 1998); and rocks damaged during the earthquake sequences (Bonini et al., 2019; Civico et al., 2018). Based on the theoretical comparison of Q, we conclude that the depth-dependent Q model has a strong effect at low to intermediate frequencies, where source parameters are estimated, and a lower effect at high frequencies ($f > 10$ Hz). Since the total attenuation of S waves traveling in a stratified crust is the product of the combined effect of Q in each layer, it is important to use Q depth-dependent corrections to evaluate ground motions generated by earthquakes.

Publisher's Note

Acknowledgements

This project was partially funded by the Mexican *Consejo Nacional de Ciencia y Tecnología* (CONACYT) project FONCICYT-CONACYT 1000/780/2016 and CONACYT Grant CB2017-2018-A1-S-37179. We thank the technical support provided by Antonio Mendoza Camberos and Arturo Pérez Vertti. We very much appreciate the careful review of the original manuscript made by Peter Klin and the anonymous reviewer. The reviewer's comments and suggestions enriched our manuscript considerably. We also thank the Associate Editor Dr. Fabio Romanelli.

References

Abercrombie, R. E. (1998). A summary of attenuation measurements from boreholes recordings of earthquakes: The 10 Hz transition problem. *Pure and Applied Geophysics, 153*, 475–487

Alvarez, W., Cocozza, T., & Wezel, F.-C. (1974). Fragmentation of the Alpine belt by microplate dispersal. *Nature, 248*(5446), 309–314

Ameri, G., Oth, A., Pilz, M., Bindi, D., Parolai, S., Luzi, L., Mucciarelli, M., & Culterra, G. (2011). Separation of source and site effects by generalized inversion technique using the aftershocks recordings of the 2009 L'Aquila earthquake. *Bulletin of Earthquake Engineering, 9*(3), 717–739

Anderson, J. G., & Hough, S. E. (1984). A model for the shape of the Fourier amplitude spectrum of acceleration at high frequencies. *Bulletin of the Seismological Society of America, 74*, 1969–1993

Andrews, D. D. (1986). Objective determination of source parameters and similarity of earthquakes of different size. In S. Dag, J. Boatwright, & C. H. Scholz (Eds.), *Earthquake Source Mechanics, Vol 37.* (pp. 259–267). Springer.

Ben-Zion, Y., & Ampuero, J. (2009). Seismic radiation from regions sustaining material damage. *Geophysical Journal International, 178*, 1351–1356

Bergamaschi, F., et al. (2011). Evaluation of site effects in the Aterno river valley (Central Italy) from aftershocks of the 2009 L'Aquila earthquake. *Bulletin of Earthquake Engineering, 9*, 697–715

Bindi, D., Castro, R. R., Franceschina, G., Luzi, L., & Pacor, F. (2004). The 1997–98 Umbria-Marche sequence (Central Italy): Source, path and site effects estimated from strong motion data recorded in the epicentral area. *Journal of Geophysical Research, 109*(B04312), 1–17

Bindi, D., Pacor, F., Luzi, L., Massa, M., & Ameri, G. (2009). The Mw 6.3, 2009 L'Aquila earthquake: Source, path and site effects from spectral analysis of strong motion data. *Geophysical Journal International, 179*, 1573–1579

Bindi, D., Spallarossa, D., & Pacor, F. (2017). Between-event and between-station variability observed in the Fourier and response spectra domains:comparison with seismological models. *Geophysical Journal International, 210*(2), 1092–1104

Bonini, L., Basili, R., Burrato, P., Cannelli, V., Fracassi, U., Maesano, F. E., et al. (2019). Testing different tectonic models for the source of the Mw 6.5, 30 October 2016, Norcia earthquke (central Italy): A youthful normal fault, or negative inversion of an old thrust? *Tectonics*. https://doi.org/10.1029/2018TC005185

Brune, J. N. (1970). Tectonic stress and the spectra of seismic shear waves from earthquake. *Journal of Geophysical Research, 75*, 4997–5009

Cara, F., Cultrera, G., Riccio, G., Amoroso, S., Bordoni, P., Bucci, A., D'Alema, E., D'Amico, M., Cantore, L., Carannante, S., Cogliano, R., Di Giulio, G., Di Naccio, D., Famiani, D., Felicetta, C., Fodarella, A., Franceschina, G., Lanzano, G., Lovati, S., … Mancini, M. (2019). Temporary dense seismic network during the 2016 Central Italy seismic emergency for microzonation studies. *Scientific Report, 6*, 182. https://doi.org/10.1038/s41597-019-0188-1

Castro, R. R., Anderson, J. G., & Singh, S. K. (1990). Site response, attenuation and source spectra of S waves along the Guerrero, México, subduction zone. *Bulletin of the Seismological Society of America, 80*, 1481–1503

Castro, R. R., & Ben-Zion, Y. (2013). Potential signatures of damage-related radiation from aftershocks of the 4 April 2010 (Mw 7.2) El Mayor-Cucapah earthquake, Baja California, México. *Bulletin of the Seismological Society of America, 103*, 1130–1140

Castro, R. R., Monachesi, G., Mucciarelli, M., Trojani, L., & Pacor, F. (1999). *P*- and S-wave attenuation in the region of Marche, Italy. *Tectonophysics, 302*, 123–132

Castro, R. R., Monachesi, G., Trojani, L., Mucciarelli, M., & Frapiccini, M. (2002). An attenuation study using earthquakes from the 1997 Umbria-Marche sequence. *Journal of Seismology, 6*, 43–59

Castro, R. R., Pacor, F., Bindi, D., Franceschina, G., & Luzi, L. (2004). Site response of strong motion stations in the Umbria, Central Italy, region. *Bulletin of the Seismological Society of America, 94*, 576–590

Castro, R. R., Pacor, F., Sala, A., & Petrungaro, C. (1996). S wave attenuation and site effects in the region of Friuli, Italy. *Journal of Geophysical Research, 101*, 22355–22369

Castro, R. R., Singh, S. K., Joshi, A., & Singh, S. (2019). Shear-wave attenuation study in the south region of the Gulf of California, Mexico. *Bulletin of the Seismological Society of America, 109*, 600–609

Castro, R. R., Trojani, L., Monachesi, G., Mucciarelli, M., & Cattaneo, M. (2000). The spectral decay parameter $_{\kappa}$ in the region of Umbria-Marche, Italy. *Journal of Geophysical Research, 105*, 23811–23823

Chiaraluce, L., Chiarabba, C., De Gori, P., Di Stefano, R., Improta, L., et al. (2011). The 2009 L'Aquila (central Italy) seismic sequence. *Bollettino di Geofisica Teorica e Applicata, 52*(3), 367–387

Chiaraluce, L., Di Stefano, R., Tinti, E., Scognamiglio, L., Michele, M., Casarotti, E., et al. (2017). The 2016 Central Italy seismic sequence: A first look at the main shocks, aftershocks, and source models. *Seismological Research Letters, 88*(3), 757–771

Civico, R., Pucci, S., Villani, F., Pizzimenti, L., De Martini, P. M., Nappi, R., & The Open EMERGEO Working Group. (2018). Surface ruptures following the 30 October 2016 Mw 6.5 Norcia earthquake, Central Italy. *Journal of Maps, 14*(2), 151–160. https://doi.org/10.1080/17445647.2018.1441756

Cultrera, G., D'Alema, E., Amoroso, S., Angioni, B., Bordoni, P., Cantore, L., Cara, F., Caserta, A., Cogliano, R., D'Amico, M., Di Giulio, G., Di Naccio, D., Famiani, D., Felicetta, C., Fodarella, A., Lovati, S., Luzi, L., Massa, M., Mercuri, A., … Mascandola, C. (2016). Site effect studies following the 2016 Mw 60 Amatrice earthquake (Italy): The Emersito task force activities. *Annals of Geophysics, 59*, 5. https://doi.org/10.4401/ag-7189

De Lorenzo, S., Bianco, F., & Del Pezzo, E. (2013). Frequency dependent Qα and Qβ in the Umbria-Marche (Italy) region using a quadratic approximation of the coda-normalization method. *Geophysical Journal International, 193*, 1726–1731

De Luca, G., Cattaneo, M., Monachesi, G., & Amato, A. (2009). Seismicity in Central and Northern Apennines integrating the Italian national and regional networks. *Tectonophysics, 476*, 121–135. https://doi.org/10.1016/j.tecto.2008.11.032

Del Pezzo, E., & Zollo, A. (1984). Attenuation of coda waves and turbidity coefficient in central Italy. *Bulletin of the Seismological Society of America, 74*, 2655–2659

Hough, S. E., Anderson, J. G., Brune, J., Vernon, F., Berger, J., Fletcher, J., Haar, L., Hanks, T., & Baker, L. (1988). Attenuation near Anza, California. *Bulletin of the Seismological Society of America, 78*(2), 672–691

Konno, K., & Ohmachi, T. (1998). Ground-motion characteristics estimated from spectral ratio between horizontal and vertical components of microtremor. *Bulletin of the Seismological Society of America, 88*(1), 228–241

Luzi, L., Pacor, F., Puglia, R., et al. (2017). The central Italy seismic sequence between August and December 2016: Analysis of strong-motion observations. *Seismological Research Letters, 88*(5), 1219–1231

Malagnini, L., Akinci, A., Mayeda, K., Munafo, I., Herrmann, R., & Mercuri, A. (2011). Characterization of earthquake-induced ground motion from the L'Aquila seismic sequence of 2009, Italy. *Geophysical Journal International, 184*, 325–337

Margheriti, L., et al. (2011). Rapid response seismic networks in Europe: Lessons learnt from the L'Aquila earthquake emergency. *Annales Geophysicae, 54*(4), 392–399

Working Group SM-AQ, 2010. Microzonazione sismica per la ricostruzione dell'area aquilana. Regione Abruzzo-Dipartimento della Protezione Civile, L'Aquila, vol. 3, e DVD-rom. http://www.protezionecivile.gov.it/jcms/it/view_pub.wp?contentId=PUB25330.

Oth, A., Bindi, D., Parolai, S., & Di Giacomo, D. (2011). Spectral analysis of K-NET and KiK- net data in Japan, Part II: On attenuation characteristics, source spectra, and site response of borehole and surface stations. *Bulletin of the Seismological Society of America, 101*, 667–687

Oth, A., Bindi, D., Parolai, S., & Wenzel, F. (2008). S-wave attenuation characteristics beneath the Vrancea region in Romania: New insights from the inversion of ground-motion spectra. *Bulletin of the Seismological Society of America, 98*, 2482–2497

Pacor, F., Spallarossa, D., Oth, A., Luzi, L., Puglia, R., Cantore, L., Mercuri, A., D'Amico, M., & Bindi, D. (2016). Spectral models for ground motion prediction in the L'Aquila región (central Italy): Evidence for stress-drop dependence on magnitude and depth. *Geophysical Journal International, 204*(2), 697–718

Parolai, S., Bindi, D., & Augliera, P. (2000). Application of the generalized inversion technique (GIT) to a microzonation study: Numerical simulations and comparison with different site-estimation techniques. *Bulletin of the Seismological Society of America, 90*, 286–297

Pauselli, D., Barchi, M., Fedeico, C., Magnani, M. B., & Minelli, G. (2006). The crustal structure of the Northern Apennines (central Italy): An insight by the Crop03 seismic line. *American Journal of Science, 306*, 428–450

Pisconti, A., Pezzo, D., Bianco, F., & de Lorenzo, S. (2015). Seismic Q estimates in Umbria Marche (central Italy): Hints for the retrieval of a new attenuation law for seismic risk. *Geophysical Journal International, 201*, 1370–1382

Priolo, E., Pacor, F., Spallarossa, D., Milana, G., Laurenzano, G., Romano, M. A., Felicetta, C., Hailemikael, S., Cara, F., Di Giulio, G., Ferretti, G., Barnaba, C., Lanzano, G., Luzi, L., D'Amico, M., Puglia, R., Scafidi, D., Barani, S., De Ferrari, R., & Cultrera, G. (2019). Seismological analyses for the seismic microzonation of the 142 municipalities damaged by the 2016–2017 seismic sequence in Central Italy. *Bulletin of Earthquake Engineering*. https://doi.org/10.1007/s10518-019-00652-x,onlineversion

Salo, T., Pugliese, R., Romero, R. W., & Marsan, P. (1998). Effetti local a Cesi (PG) durante la sequenza sísmica del Settembre-Ottobre 1997. *Ingenieria Sísmica, 3*, 14–20

Singh, S. K., Apsel, R. J., Fried, J., & Brune, J. N. (1982). Spectral attenuation of SH waves along the Imperial fault. *Bulletin of the Seismological Society of America, 72*, 2003–2016

Singh, S. K., & Ordaz, M. (1994). Seismic energy release in Mexican subduction zone earthquakes. *Bulletin of the Seismological Society of America, 84*, 1533–1550

Vai, G. B. (2001). Structure and stratigraphy: An overview. In G. B. Vai & I. P. Martini (Eds.), *Anatomy of an Orogen: The Apennines and Adjacent Mediterranean Basins.* (pp. 15–32). Kluwer Academic Publishing.

Valoroso, L., Chiaraluce, L., Piccinini, D., Di Stefano, R., Schaff, D., & Waldhauser, F. (2013). Radiography of a normal fault system by 64,000 high-precision earthquake locations: The 2009 L'Aquila (central-Italy) case study. *Journal of Geophysical Research, 118*(3), 1156–1176